Equilibrium properties and phase diagram of two-dimensional Yukawa systems

P. Hartmann,[1] G. J. Kalman,[2] Z. Donkó,[1] and K. Kutasi[1]

[1]*Research Institute for Solid State Physics and Optics of the Hungarian Academy of Sciences, H-1525 Budapest, P.O. Box 49, Hungary*
[2]*Department of Physics, Boston College, Chestnut Hill, Massachusetts 02467, USA*
(Received 26 April 2005; published 22 August 2005)

Properties of two-dimensional strongly coupled Yukawa systems are explored through molecular dynamics simulations. An effective coupling coefficient Γ^* for the liquid phase is introduced on the basis of the constancy of the first peak amplitude of the pair-correlation functions. Thermodynamic quantities are calculated from the pair-correlation function. The solid-liquid transition of the system is investigated through the analysis of the bond-angular order parameter. The static structure function satisfies consistency relation, attesting to the reliability of the computational method. The response is shown to be governed by the correlational part of the inverse compressibility. An analysis of the velocity autocorrelation demonstrates that this latter also exhibits a universal behavior.

PACS number(s): 52.27.Gr, 05.20.−y, 73.21.−b

I. INTRODUCTION

The Yukawa (screened Coulomb) potential is a widely used approximation to describe the interaction of particles in a variety of physical systems, e.g., dusty plasmas in laboratory [1] and space [2] and charged colloids [3]. The Yukawa interaction potential (energy) is $\phi(r) = (Q^2/r)\exp(-\kappa r)$. Many-particle systems with Yukawa interaction can fully be characterized by two dimensionless parameters: (i) the *coupling parameter* $\Gamma = \beta Q^2/a$ (where Q is the charge of the particles, a is the Wigner–Seitz radius, and $\beta = 1/k_B T$ is the inverse temperature), and (ii) the *screening parameter* $\bar{\kappa} = \kappa a$.

Besides three-dimensional (3D) systems, two-dimensional (2D) configurations also appear in a wide variety of physical systems. As examples of such Coulomb or Yukawa systems, respectively, the layer of electrons on the surface of liquid helium or layers of dust particles formed in low-pressure gas discharges may be mentioned [4–8]. The dynamics of these 2D systems has extensively been investigated both theoretically and by simulation techniques, e.g., [9–12], but much less so insofar as the study of the equilibrium properties of such systems is concerned (see, however, a recent paper by Totsuji *et al.* [10] and [13–15]). This paper addresses this latter issue: we report on molecular-dynamics (MD) simulations through which various equilibrium properties of a 2D Yukawa system are explored. In Sec. II we describe our simulation technique. In Sec. III we display pair-correlation functions and show how most of the equilibrium properties of a 2D Yukawa system can be described in terms of an effective coupling parameter. In Secs. IV and V, respectively, we calculate the energy and pressure, and display the phase boundary between the liquid and solid phases. Sections VI and VII are devoted to the related issues of the static structure factor, the static dielectric function, and the behavior of the isothermal compressibility. Finally, in Sec. VIII we present simulation results for the velocity autocorrelation function and provide a qualitative explanation of its observed features.

II. SIMULATION TECHNIQUE

The motion of the particles is traced by molecular-dynamics technique based on the PPPM (particle-particle particle-mesh) algorithm [16], which allows efficient simulation of systems composed of a large number of particles [17]. We use a variant of the method modified for a Yukawa potential. The simulation domain is a three-dimensional cubic box with periodic boundary conditions in which the particles are constrained to move within a two-dimensional layer. In the PPPM method the interparticle force is partitioned into (i) a force component F_{PM} that can be calculated on a mesh (the "mesh force") and (ii) a short-range force F_{PP}, which is to be applied to closely separated pairs of particles only (for more details see [16]). In this way the PPPM method makes it possible to take into account periodic images of the system (in the PM part), without truncating the long-range Coulomb or low-$\bar{\kappa}$ Yukawa potentials. (For high $\bar{\kappa}$ values the PP part alone provides sufficient accuracy, in these cases the mesh part of the calculation is not used.) In most simulations, the desired system temperature is reached by rescaling the particle momenta during the initialization phase of the simulation. The system temperature does not show an observable drift during the subsequent measurement phase of the simulation that follows the initialization period. In the simulations aimed at the determination of the solid-liquid phase boundary the Nosé–Hoover thermostat (e.g., [18]) is used to ensure a correct control of the system temperature.

The primary output data of our simulations are the pair-correlation functions (PCFs) $g(r)$, which contain indispensable information about the system [19]. The PCFs are used as input data for the calculation of the correlational energy, pressure, and compressibility of the system, and for the calculation of the static structure function $S(k)$ as well. Additional quantities, e.g., velocity autocorrelation functions (VACF) are also analyzed. The solid-to-liquid transition is studied through monitoring the temperature dependence of the bond-angular order parameter (see below).

Our simulations also provide information about the spectra of the longitudinal and transverse current fluctuations in

the liquid phase of the system where isotropy can be assumed [11]. These spectra are obtained through the Fourier transform [20,21]

$$L(k,\omega) = |\mathcal{F}\{\lambda(k,t)\}|^2,$$

$$T(k,\omega) = |\mathcal{F}\{\tau(k,t)\}|^2, \qquad (1)$$

of the microscopic quantities

$$\lambda(k,t) = k\sum_j v_{jx}\exp(ikx_j),$$

$$\tau(k,t) = k\sum_j v_{jy}\exp(ikx_j), \qquad (2)$$

where the index j runs over all particles.

The spectra defined by (1) serve as the basis for the analysis of the collective excitations of the system. We have reported detailed calculations on this topic in [11].

In the following, the simulation results are given with the length scale normalized by the 2D Wigner–Seitz radius $a = 1/\sqrt{n\pi}$ (where n is the areal density), i.e., $\bar{r} = r/a$ and $\bar{k} = ka$.

III. SCALING

The issue of scaling (i.e., whether only some combination of the Γ and $\bar{\kappa}$ parameters rather than both of these parameters independently or, alternatively, the ratio of the temperature to the melting temperature govern the behavior of Yukawa systems) has been addressed by several studies; the universal scaling of structural properties and transport parameters has continued to receive attention for many years [22–29].

In the case of three-dimensional Yukawa systems, the suggestion for an *effective coupling parameter* $\Gamma^* = \Gamma\exp(-\bar{\kappa})$ was given by Ikezi [30] and was based on the argument that the coupling for a Yukawa potential is obtained from the Coulomb coupling parameter by multiplying the latter by $\exp(-\bar{\kappa}\bar{r})$. Subsequent studies, however, have shown that different systems characterized by the same Γ^* do not show many similarities. [According to our 2D simulations, at certain values of $\Gamma^* = \Gamma\exp(-\bar{\kappa})$ (e.g., 120), the system may be either in the liquid or in the solid phase, depending on the value of $\bar{\kappa}$.] A more recent and more meaningful definition for the effective coupling parameter was given by Vaulina, *et al.* [25], Vaulina and Vladimirov [26], and Fortov *et al.*[27]. Their definition of Γ^* is based on the frequency of dust lattice waves, resulting in $\Gamma^* = \Gamma(1+\bar{\kappa}+\bar{\kappa}^2/2)\exp(-\bar{\kappa})$. They have shown that within the $0 \le \bar{\kappa} \le 5$ range, their effective coupling parameter has a nearly constant value $\Gamma^* = \Gamma_m^{3D}$ (where $\Gamma_m^{3D} \cong 175$ is the coupling coefficient value at which the 3D one-component plasma melts) along the solid-liquid phase boundary determined by Hamaguchi *et al.* [31]. Moreover, it was also demonstrated [27] that systems with the same Γ^* value have very similar pair-correlation functions [25–27]. In our earlier work [11] we considered defining an effective coupling parameter for a two-dimensional Yukawa system. We established a different criterion for Γ^* that relies
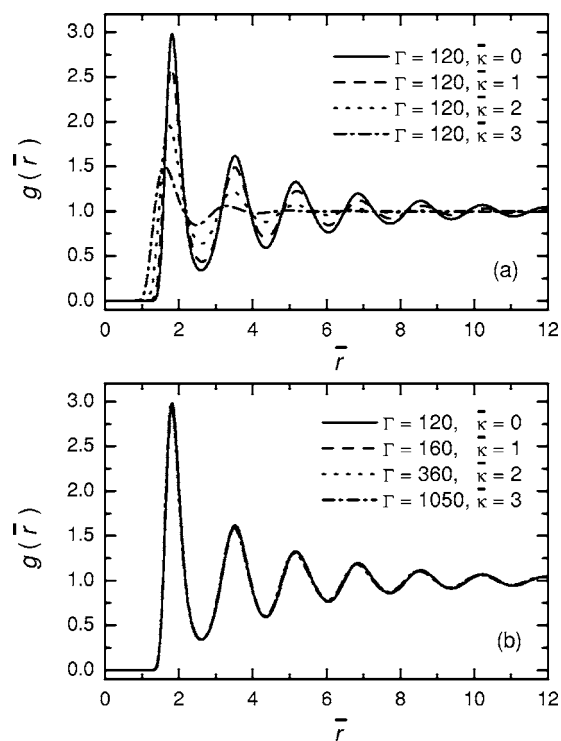

FIG. 1. Pair-correlation functions vs distance in units of the Wigner-Seitz distance a of the 2D Yukawa liquid for (a) $\Gamma = 120$ and different values of $\bar{\kappa}$, and (b) for a series of $(\Gamma,\bar{\kappa})$ pairs corresponding to a constant $\Gamma^* = 120$.

on associating a constant amplitude of the first peak of the PCF [$g(r)$] with a constant Γ^* value.

Our aim now is to find a proper $f(\bar{\kappa})$ function that allows one to partition $\Gamma^*(\Gamma,\bar{\kappa})$ as

$$\Gamma^* = \Gamma f(\bar{\kappa}). \qquad (3)$$

In order to obtain the $f(\bar{\kappa})$ function we have carried out an extensive scan of the PCFs over a wide domain of the $(\Gamma,\bar{\kappa})$ parameter space. The pair-correlation functions of the 2D Yukawa liquid are displayed in Fig. 1(a) for $\Gamma = 120$ and for a series of $\bar{\kappa}$ values. It can be seen that the range of the rather pronounced order characteristic for $\bar{\kappa} = 0$ rapidly diminishes with increasing $\bar{\kappa}$. The amplitude of the first peak of the PCF can, however, be reestablished if Γ is also increased together with $\bar{\kappa}$. This is illustrated in Fig. 1(b). In fact, as Fig. 1(b) shows, within the range of $\bar{r}$ displayed not only the amplitude of the first peak, but the $g(\bar{r})$ functions in their entireties are nearly the same for fixed Γ^* values, even though the associated $\bar{\kappa}$ values are quite different. A caveat, however, has to be added. As it is discussed below, the values of the static structure function $S(k)$ at $k = 0$ are sensitive to the variation of $\bar{\kappa}$, even at $\Gamma^* = $ constant values. Since $S(k=0) = 1 + n\int h(r)d\mathbf{r}$ [where $h(r) = g(r) - 1$ and $\mathbf{r}$ lies in the particle plane], the difference must come from the tail of $g(r)$, which is, apparently "unscalable" and the scaling property of $g(r)$ cannot extend to $r \to \infty$.

Figure 2(a) shows the contours on the $\Gamma - \bar{\kappa}$ plane that belong to constant effective coupling values $\Gamma^* = 120$, 40, and
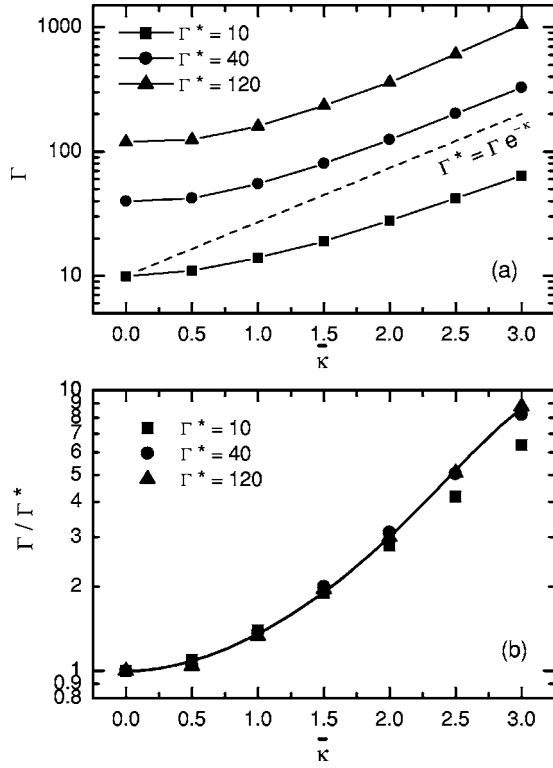
FIG. 2. (a) Constant effective coupling (Γ^*) lines on the $\Gamma - \bar{\kappa}$ plane. The dashed line represents Ikezi's definition $\Gamma^* = \Gamma \exp(-\bar{\kappa})$ for $\Gamma^* = 10$. (b) Dependence of the ratio Γ/Γ^* on $\bar{\kappa}$. The symbols are data taken from (a), while the solid line is a fit according to (3) and (4).
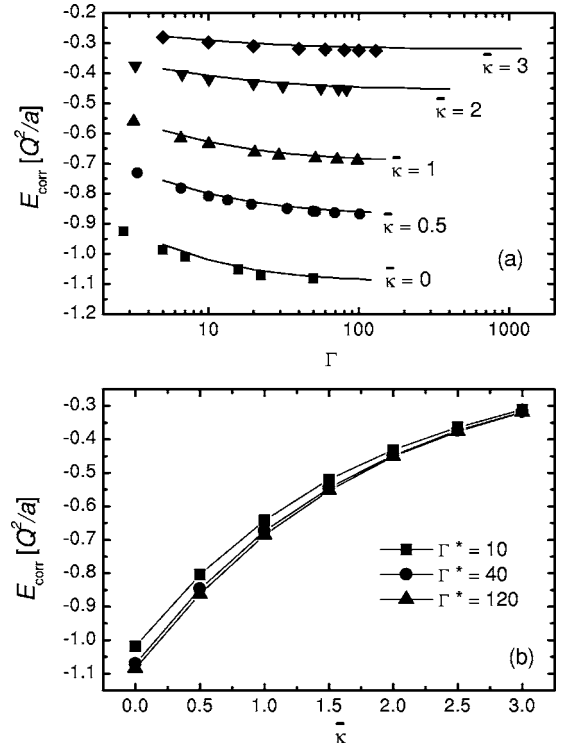

FIG. 3. (a) Correlation energy per particle of the 2D Yukawa liquid as a function of Γ, for selected values of $\bar{\kappa}$. Lines: present results, symbols: data of Totsuji *et al.* [10]. (b) Correlation energy per particle as a function of $\bar{\kappa}$, for constant values of the effective coupling parameter Γ^*.

10. It can be seen that these lines have approximately the same shape; thus, they can be scaled to a single universal line, as shown in Fig. 2(b), which displays the dependence of the ratio Γ/Γ^* on $\bar{\kappa}$ for the chosen values of Γ^*. At high values of Γ^*, the ratio Γ/Γ^* depends only on $\bar{\kappa}$, the partitioning given in (3) is indeed possible, and $f(\bar{\kappa})$ can be fitted with the aid of the following:

$$f(\bar{\kappa}) = 1 + f_2 \bar{\kappa}^2 + f_3 \bar{\kappa}^3 + f_4 \bar{\kappa}^4, \quad \text{with}$$

$$f_2 = -0.388; \quad f_3 = 0.138; \quad f_4 = -0.0138. \tag{4}$$

It can be seen in Fig. 2(b) that the results can accurately be represented by Eq. (4) except for the lowest $\Gamma^* = 10$ value.

IV. THERMODYNAMIC QUANTITIES

The energy (per particle) of the system E consists of the thermal part E_0, the positive Hartree part E_H, and the negative correlational part E_c:

$$\beta E_0 = 1$$

$$\beta E_H = \beta \frac{n}{2} \int \phi(r) \mathrm{d}\mathbf{r} = \beta \frac{Q^2 \pi n}{\kappa} = \frac{\Gamma}{\bar{\kappa}}$$

$$\beta E_c = \beta \frac{n}{2} \int h(r) \phi(r) \mathrm{d}\mathbf{r} = \Gamma \int_0^\infty h(\bar{r}) e^{-\bar{\kappa} \bar{r}} \mathrm{d}\bar{r}. \tag{5}$$

Similarly, the pressure consists of the ideal, the positive Hartree and the negative correlational contributions

$$\beta P_0 = n$$

$$\beta P_H = \beta \frac{n^2}{2} \int \phi(r) \mathrm{d}\mathbf{r} = \frac{\pi Q^2 n^2}{\kappa} = \beta \frac{\Gamma}{\bar{\kappa}} n$$

$$\beta P_c = -\beta \frac{n^2}{4} \int r \frac{\partial \phi(r)}{\partial r} h(r) \mathrm{d}\mathbf{r} = \frac{n \Gamma}{2} \int_0^\infty \bar{r} \left[\bar{\kappa} + \frac{1}{r} \right] e^{-\bar{\kappa} \bar{r}} h(\bar{r}) \mathrm{d}\bar{r}. \tag{6}$$

The correlation energy per particle [calculated according to (5)] and the correlational part of the pressure [calculated according to (6)] can now be obtained from the PCF. The former is plotted in Fig. 3(a) as a function of Γ, for different values of $\bar{\kappa}$. Plotting the same data as a function of $\bar{\kappa}$ for constant values of Γ^* shows that E_c depends only slightly on Γ^* in the strong coupling domain, but varies strongly with $\bar{\kappa}$, as expected, since only $h(r)$—but not $\phi(r)$—is scaled within the integral. The data can be approximated as

$$\beta E_c = \Gamma [b(\bar{\kappa}) + c(\bar{\kappa}) \Gamma^{*-2/3}], \quad \text{with}$$

$$b(\bar{\kappa}) = b_0 + b_1 \bar{\kappa} + b_2 \bar{\kappa}^2 + b_3 \bar{\kappa}^3 + b_4 \bar{\kappa}^4, \quad \text{and}$$
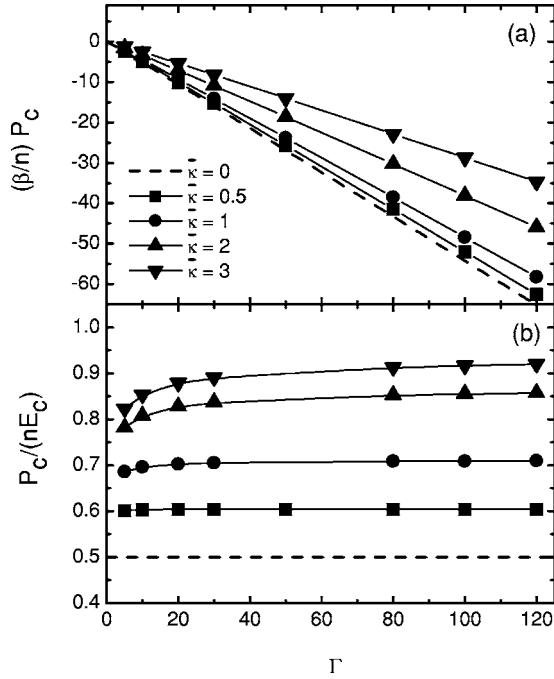
FIG. 4. (a) Correlational part of the pressure $(\beta P_c/n)$ as a function of Γ for $\bar{\kappa}=0.5$, 1, 2, and 3. The dashed line shows the theoretical behavior of the pure Coulomb OCP. (b) The ratio $P_c/(nE_c)$ as a function of Γ.

$$c(\bar{\kappa}) = c_0 + c_1\bar{\kappa} + c_2\bar{\kappa}^2 + c_3\bar{\kappa}^3 + c_4\bar{\kappa}^4, \qquad (7)$$

where $b_0=-1.103$; $b_1=0.505$; $b_2=-0.107$; $b_3=0.00686$; $b_4=0.0005$ and $c_0=0.384$; $c_1=-0.036$; $c_2=-0.052$; $c_3=0.0176$; $c_4=0.00165$.

Our data shown in Fig. 3(a) are in an excellent agreement with the energy values recently calculated by Totsuji *et al.* [10] and at $\kappa=0$ with the energy values given for the 2D one-component plasma (OCP) [5,10,32].

The correlational part of the pressure is plotted in Fig. 4(a) as a function of Γ, for different values of $\bar{\kappa}$. Similarly to the energy, the data are in an excellent agreement with those of Totsuji *et al.* [10]. In the $5 \leqslant \Gamma \leqslant 120$ and $0.5 \leqslant \bar{\kappa} \leqslant 3$ interval the correlational part of the pressure (P_c) can be fitted using the form

$$\beta P_c = n\Gamma(b_0' + b_1'\bar{\kappa}), \qquad (8)$$

where $b_0'=-0.5638$ and $b_1'=0.09367$.

It is interesting to note that while in the Coulomb case the pressure and the energy are linked through the virial theorem as $P_c=\frac{1}{2}nE_c$, no such relationship exists for $\bar{\kappa} \neq 0$ [see (6) and Fig. 4(b)].

V. PHASE DIAGRAM

The issue of the number of distinct phases in a 2D Coulomb or Yukawa systems has been, for some time, a matter of intense controversy [33]. The Kosterlitz–Thouless–Halperin–Nelson–Young (KTHNY) theory of the 1970s (see, e.g., [34]) suggested that in the course of the transition from the liquid phase to the crystalline phase with quasi-long-range
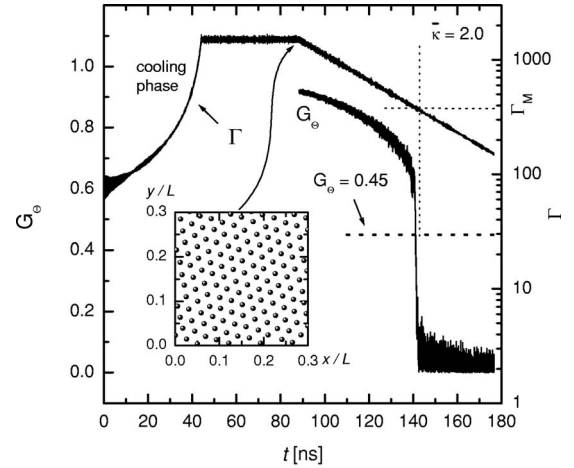

FIG. 5. Illustration of the "melting experiment:" time dependence of the bond-angular order parameter G_Θ and system temperature T, obtained at $\bar{\kappa}=2$. The sudden decay of G_Θ below the 0.45 value [36]—marking the solid → liquid transition—occurs at $\Gamma_m=384$. The inset shows a snapshot of particle positions recorded right before the temperature starts to increase.

positional order and a long-range orientational order, an intermediate "hexatic" phase exists without a long-range positional order but dominated by a quasi-long-range orientational order.

The transitions between the different phases can be characterized by the behavior of the bond-angular order parameter G_Θ (e.g., [35]). For a system with hexagonal symmetry, the bond-angular order parameter [35,36] has the form

$$G_\Theta = \frac{1}{N}\left|\sum_{k=1}^{N}\frac{1}{6}\sum_{m=1}^{6}\exp(i6\Theta_{k,m})\right|^2, \qquad (9)$$

where the indices k runs over all particles of the system, m runs over the six nearest neighbors neighbors of the kth particle, and $\Theta_{k,m}$ is the angle between a predefined (e.g., x) direction and the vector connecting the kth and mth particles. For the determination of the solid-liquid phase diagram we follow Schweigert *et al.* [36] who investigated systems characterized by different interaction potentials and inferred that the solid-to-liquid transition can be identified by a drop of the bond-angular order parameter below a value of $G_\Theta \cong 0.45$; (see also [13,14]).

The melting "experiment" of the 2D Yukawa layer is illustrated in Fig. 5. At the beginning of the simulation, a particle configuration with random particle positions is initialized with an initial temperature well above the expected value of melting temperature. The temperature of the system is slowly decreased afterward, and ample time is given to the system to reach an ordered configuration (as shown in the inset of Fig. 5). Subsequently, the temperature is slowly increased and the bond-angular order parameter G_Θ is calculated according to (9) in each time step. As a consequence of the increasing temperature, first we observe a slow decay of G_Θ (from an initial value close to 1.0, indicating nearly perfect hexagonal order) and later on, when the temperature reaches a certain value, G_Θ suddenly drops to ≈ 0, indicating

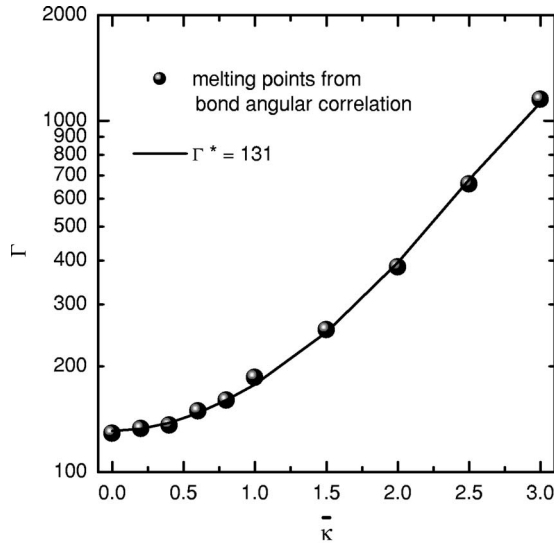FIG. 6. Γ_m as a function of $\bar{\kappa}$ as obtained from the "melting experiments" (symbols) and the $\Gamma^*=131$ line.

an abrupt loss of the long-range orientational order in the system. We identify this event, taking place at $\Gamma=\Gamma_m$, as the solid to liquid transition. The temperature control of the system is realized by the Nosé–Hoover algorithm (see, e.g., [18]). To obtain the $\Gamma_m-\bar{\kappa}$ phase diagram of the system, the simulations are carried out for a series of screening parameter values. All results presented here have been obtained using $N=1600$ particles.

The $\Gamma_m-\bar{\kappa}$ phase boundary obtained from simulations illustrated above is plotted in Fig. 6. At $\bar{\kappa}=0$ the simulations closely reproduce the well-known value $\Gamma_m^{Coulomb} \cong 137$ for the 2D OCP. The figure also shows the Γ values calculated from (4), assuming $\Gamma^*=131$. We find an excellent agreement between the two sets of data. This agreement shows that the first peak amplitude of the PCF is nearly constant along the melting line of 2D Yukawa systems, regardless of the value of $\bar{\kappa}$, as already pointed out before. Studies of Vaulina *et al.* [25], and Vaulina and Vladimirov [26], and Fortov *et al.* [27] have actually reached a similar conclusion for 3D Yukawa systems.

An early attempt to theoretically determine the solid-liquid phase boundary for a 2D Yukawa system is due to Peeters and Wu [15]. Their calculation is based on the KTHNY theory of dislocation-mediated melting [34,35]. The structure of the phase diagram obtained in this work is not corroborated by our MD results: Peeters and Wu [15] find a significantly ($\approx40\%$) lower melting Γ than is shown in Fig. 6. The possible presence of a hexatic phase (as predicted by the KTHNY theory) was not investigated in [15].

VI. STATIC STRUCTURE FUNCTION

The static structure function is derived from the PCFs as

$$S(k) = 1 + 2\pi n \int_0^\infty h(r) r J_0(kr) dr. \tag{10}$$
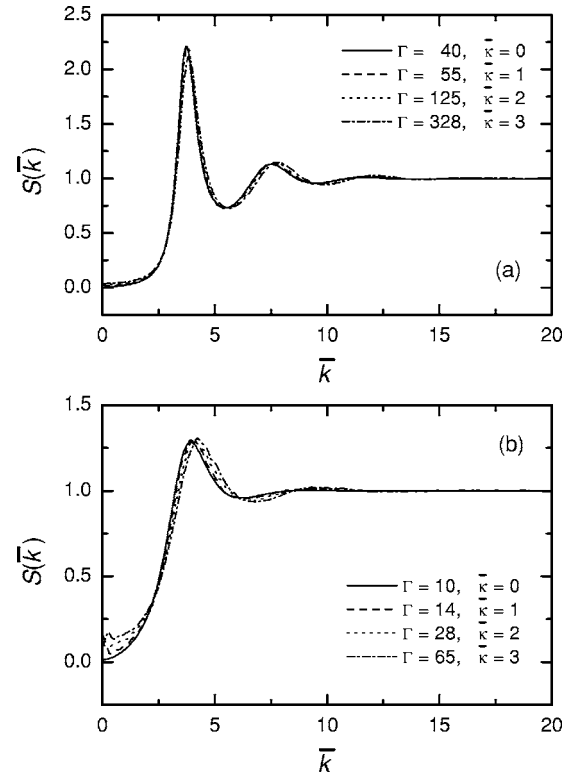

FIG. 7. Static structure functions of the 2D Yukawa liquid for (a) $\Gamma^*=40$ and (b) $\Gamma^*=10$.

Representative plots of $S(k)$ obtained from the PCF through (10) are displayed in Figs. 7(a) and 7(b) for the $\Gamma^*=40$ and 10 values, respectively. As the $S(k)$ functions are derived from the PCFs we expect the $S(k)$ functions belonging to the same Γ^* to show similarity. On the other hand, $S(k=0)$ is expected to increase with increasing $\bar{\kappa}$: for the Coulomb case $S(k=0)=0$, whereas Yukawa systems are characterized by $S(k=0)>0$. As this effect is also emphasized with decreasing Γ, the increase of $S(k=0)$ is clearly observed in the case of $\Gamma^*=10$, while it is less pronounced at $\Gamma^*=40$.

The value of $S(k)$ for $k \to 0$ is governed by the compressibility sum rule for $\bar{\chi}$, the "screened" (total) static density response function, which can be written in the form

$$\bar{\chi}(k \to 0) = - \frac{\beta n}{1 + L_c + M\bar{k}^2}, \tag{11}$$

where L_c is the correlational part of the inverse compressibility and M represents the correlation-induced contribution of $O(k^2)$ in the $\bar{\chi}(k \to 0)$ expansion. From the fluctuation-dissipation relationship

$$S(k) = - \frac{\bar{\chi}(k)/\beta n}{1 - \phi(k)\bar{\chi}(k)} \tag{12}$$

[$\phi(k)=2\pi Q^2/\sqrt{\kappa^2+k^2}$ is the Fourier transform of the Yukawa potential energy], one finds

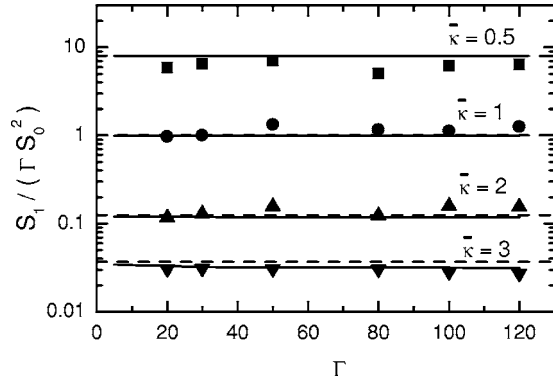$$S(\bar{k}) = S_0 + S_2\bar{k}^2, \quad \text{where}$$

FIG. 8. Ratio of the zeroth- and second-order terms of the static structure function $S(k \rightarrow 0)$ expansion. Plotted are the values of the $S_1/S_0^2\Gamma$ expression as functions of Γ for $\bar{\kappa}=0.5$, 1, 2, and 3. The lines show the predictions of the QLCA theory [the dashed lines show calculations ignoring term e in (13)].

$$S_0 = \left(\frac{2\Gamma}{\bar{\kappa}} + 1 + L_c\right)^{-1} \quad \text{and}$$

$$S_2 = \frac{2\Gamma}{\left(\frac{2\Gamma}{\bar{\kappa}} + 1 + L_c\right)^2} \left(\frac{1}{2\bar{\kappa}^3} - e\right). \tag{13}$$

The constant e appearing in (13) is linked to the M coefficient in (11) and, as such, cannot be predicted without adopting some model for the dynamics of the strongly coupled systems. If we espouse the extended version of the quasilocalized charge approximation (QLCA) that allows the analysis of the static response [37], e can be identified as the coefficient of the $O(k^4)$ term in the dynamical matrix $D(\mathbf{k})$ [11], i.e.,

$$\frac{D(\mathbf{k})}{k^2} \rightarrow \omega_p^2 a^2(-d + e\bar{k}^2). \tag{14}$$

Our calculations show that e is small in comparison to the other terms in (13), and its precise value does not substantially affect the results of calculations ensuing from (13). Nevertheless, a comparison of the S_0 and S_2 coefficients (see Fig. 8) shows that inserting the QLCA value of e in S_2 well reproduces the relationship between S_0 and S_2 as required by (13).

The correlational part of the inverse compressibility L_c is obtained from the pressure through the relation $L_c = \beta(\partial P_c/\partial n)$. Based on the fitting formula (8) L_c becomes

$$L_c = \beta\frac{\partial P_c}{\partial n} = \left(\frac{3}{2}b_0' + b_1'\bar{\kappa}\right)\Gamma = (-0.8458 + 0.09367\bar{\kappa})\Gamma. \tag{15}$$

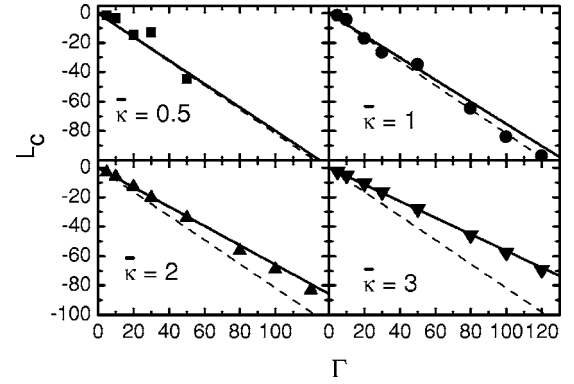If, on the other hand, the static structure function is known, L_c can be determined directly from $S_0 = S(k=0)$ as

FIG. 9. Correlational inverse compressibility L_C as a function of Γ for different $\bar{\kappa}$ values. Lines show data based on the equation-of-state calculation [through (15)] and symbols show points calculated using the structure function $S(k)$ [through (16)]. The dashed lines show the theoretical behavior of the pure Coulombic OCP.

$$L_c = \frac{1}{S_0} - \frac{2\Gamma}{\bar{\kappa}} - 1. \tag{16}$$

We note that the difficulty in this latter method is the strong dependence of $S(k)$ for small k values on the fluctuations appearing in the simulation due to the finite number of particles. This makes long runs and extensive averaging necessary to achieve data with an acceptable level of scattering.

The comparison of the results obtained from the two independent methods provides an important check on the consistency and accuracy of the computation. The outcomes of the two calculations are compared in Fig. 9. A strong coincidence of the two sets of results, especially for larger $\bar{\kappa}$ values, verifies the consistency of the computational procedure.

Figure 9 shows that the absolute value of the (negative) L_c decreases with increasing $\bar{\kappa}$ values. We note that, in any case, the total compressibility includes the Hartree term L_H, and is always positive, as required by the usual equilibrium stability criterion.

VII. DIELECTRIC FUNCTION

The static dielectric function $\varepsilon(k)$ is an important quantity governing the screening of an impurity and the tendency of the system to develop charge-density waves. It is obtained from $S(k)$ via the fluctuation-dissipation relation (11) by identifying

$$\varepsilon(k) = 1 - \phi(k)\bar{\chi}(k), \tag{17}$$

thus providing

$$\varepsilon(k) = \frac{1}{1 - 2\Gamma\frac{1}{\sqrt{\bar{k}^2 + \bar{\kappa}^2}}S(k)}. \tag{18}$$

Figure 10 shows the behavior of the static $\varepsilon(k)$ for various combinations of Γ and $\bar{\kappa}$ values. For high Γ values $\varepsilon(k)$ exhibits the familiar "inverted U" behavior characteristic for
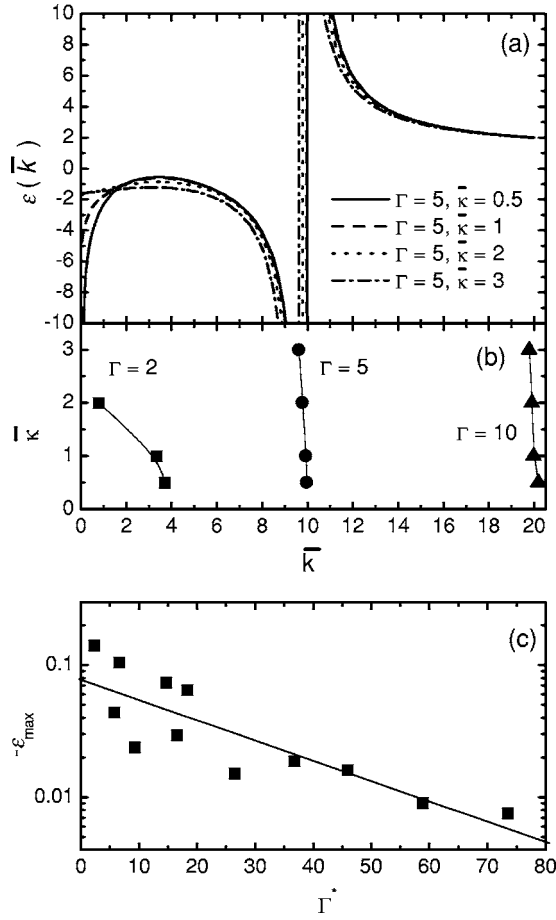
FIG. 11. (a–d) Velocity autocorrelation functions obtained at $\Gamma^* = 120$ and a series of $\bar{\kappa}$ values (ω_p is the nominal 2D plasma frequency). (e) The same data replotted against time normalized by the ($\bar{\kappa}$-dependent) Einstein frequency ω_E.

$$Z(t) = \frac{\langle \mathbf{v}(t)\mathbf{v}(0) \rangle}{\langle |\mathbf{v}(0)|^2 \rangle}, \qquad (19)$$

where the average is taken over the N particles and different initial times.

Representative velocity autocorrelation functions (VACF) (19) obtained at $\Gamma^* = 120$ for series of $\bar{\kappa}$ values are displayed in Figs. 11(a)–11(d). The $Z(t)$ functions (plotted against $\omega_p t$) exhibit marked oscillations. Here $\omega_p = \sqrt{2\pi Q^2 n / ma}$ is the nominal 2D plasma frequency. Such marked oscillations with a period nearly independent of Γ in the two-dimensional strongly coupled classical electron layer—similar to those of the three-dimensional one-component plasma [39]—have already been found by Kalia *et al.* [40] and Hansen *et al.* [41]. In the 3D case the oscillations of the VACFs were indeed expected on the basis of the possible coupling between the single particle motion and long-wavelength plasmons whose frequencies are almost independent of k. In 2D, in contrast, it is well known that the plasmon frequency (ω) depends on the wave number k and in the limit of $k \to 0$ the mode frequency $\omega \to 0$. The $\omega(k)$ dispersion curve, however, flattens at higher wave numbers, and this latter behavior has been identified to lead to an appreciable coupling between the single particle motion and collective excitations.

Our results show that the dominant frequency in the Coulomb case amounts $\omega \cong 0.9 \; \omega_p$ [Fig. 11(a)], and this value decreases with increasing $\bar{\kappa}$ [Figs. 11(b)–11(d)]. Figure 11(e) shows the $Z(t)$ functions replotted against $\omega_E t$ instead of $\omega_p t$, where ω_E is the Einstein frequency, defined as the oscillation frequency of a test particle in the frozen environment of all other particles situated at lattice sites. ω_E as a function of $\bar{\kappa}$ is

FIG. 10. (a) Dielectric function $\varepsilon(k)$ for $\Gamma = 5$, $\bar{\kappa} = 0.5$, 1, 2, and 3. (b) The position of the singularity $\bar{k}_{\mathrm{pole}}$ of $\varepsilon(\bar{k})$ for low Γ values. (c) The negative maximum of $\varepsilon(\bar{k})$ as a function of Γ^*.

strongly coupled Coulomb systems (see, e.g., [37]), with a negative pole around $\bar{k} \approx 2\Gamma$. In contrast to Coulomb systems, however, $\varepsilon(k=0)$ is finite and its value is governed by the value of L_c.

With increasing Γ^* values, the maximum of $\varepsilon(k)$ in the inverted-U region approaches zero (see Fig. 10). This indicates the tendency of the system to develop charge-density waves, i.e., an oscillatory screening response to an impurity [38].

The position of the singularity $\bar{k}_{\mathrm{pole}}$ of $\varepsilon(\bar{k})$ for low Γ values and the negative maximum of $\varepsilon(\bar{k})$ as a function of Γ^* are displayed in Figs. 10(b) and 10(c). From (11) and (17) it is not difficult to show that the pole at $\bar{k} = \bar{k}^*$ disappears and $\varepsilon(\bar{k})$ becomes a monotonic positive definite function of $\bar{k}$ for Γ values where $1 + L_c \geq 0$.

VIII. VELOCITY AUTOCORRELATION FUNCTION

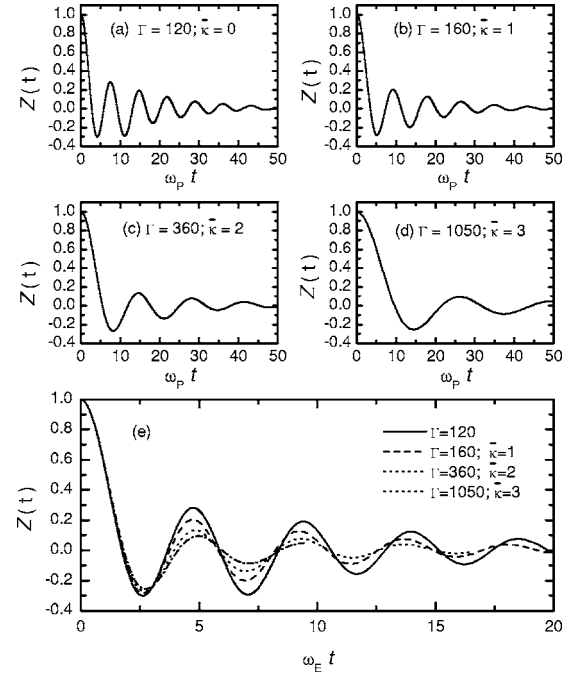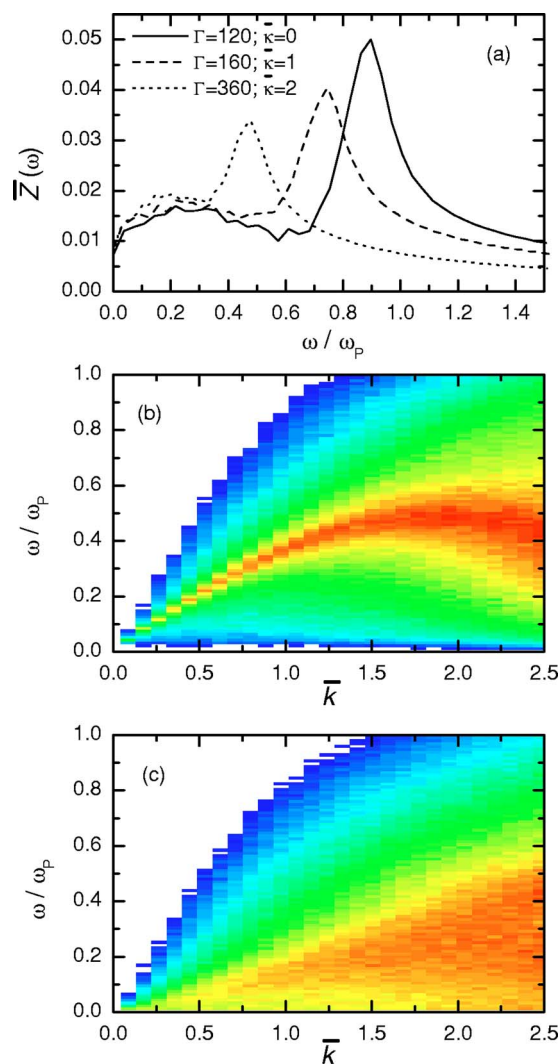The velocity autocorrelation function $Z(t)$ is obtained according to

FIG. 12. (Color online) (a) Fourier transforms $\bar{Z}(\omega)$ of the VACFs obtained at $\Gamma^* = 120$, for selected values of $\bar{\kappa}$. (b) longitudinal $L(\bar{k}, \omega)$ and (c) transverse $T(\bar{k}, \omega)$ current fluctuations obtained at $\Gamma = 360$, $\bar{\kappa} = 2$. (The color coding of the amplitude is logarithmic; it only intends to illustrate qualitative features.)

obtained from a formula based on the QLCA method [42], using MD-generated pair-correlation functions. Figure 11(e) shows that the oscillation frequency (when given in units of ω_E) is nearly independent of $\bar{\kappa}$ and in the vicinity of $\omega \cong 1.3\, \omega_E$, indicating a universality of the dynamical behavior of the systems investigated.

The Fourier transforms $\bar{Z}(\omega)$ of the VACFs shown in Figs. 11(a)–11(c) are portrayed in Fig. 12(a). The dominant peaks in the spectra, shifting toward lower frequencies with increasing $\bar{\kappa}$, correspond to the high-frequency oscillations of the $Z(t)$ functions (easily observed visually). As discussed in previous studies (see, e.g., [23,43]), these peaks are related to longitudinal current fluctuations, while the broad features at low frequencies are connected to the (slower) decay of $Z(t)$.

The latter characterize the transverse current fluctuations and are related to diffusion properties of the system. The spectra of the longitudinal and transverse current fluctuations, $L(\bar{k}, \omega)$ and $T(\bar{k}, \omega)$, respectively, are displayed in the form of color maps in Figs. 12(b) and 12(c), for the $\Gamma = 360$, $\bar{\kappa} = 2$ case. The spectra of the longitudinal current fluctuations show that at small $\bar{k}$ the mode frequency increases linearly with $\bar{k}$, then within a relatively wide range of $\bar{k}$ the mode frequency in near to $\omega/\omega_p \approx 0.45$, in correspondence with the peak of $\bar{Z}(\omega)$ shown in Fig. 12(a). The $T(\bar{k}, \omega)$ spectra [see Fig. 12(c)] for any $\bar{k}$ are broader, compared to the $L(\bar{k}, \omega)$ spectra; the fluctuations in the transverse currents are distributed over a rather broad frequency domain, again in agreement with the behavior of the corresponding $\bar{Z}(\omega)$ function. The observed features of $\bar{Z}(\omega)$ indeed support the model of coupling between single particle motion and collective excitations in the 2D system.

IX. SUMMARY

Two-dimensional strongly coupled Yukawa systems have been investigated by molecular-dynamics simulations. We have shown that an effective coupling coefficient Γ^* can be defined, based on the constancy of the first peak amplitude of pair-correlation functions (PCFs). It was demonstrated that systems characterized by different $(\Gamma, \bar{\kappa})$ pairs belonging to the same Γ^* have very nearly the same PCFs. We have calculated thermodynamic quantities and have found good agreement with recent theoretical calculations [10].

The results of "melting experiments" on systems characterized by a wide range of the screening parameter $\bar{\kappa}$ showed that the solid-liquid phase boundary can be given by $\Gamma^* = \Gamma_m^{OCP}$ to a good approximation.

The satisfaction of theoretically established relationships between the static structure function $S(k)$ and the correlational inverse compressibility L_c has been verified, indicating the high degree of reliability of the computational procedure. We have analyzed the ensuing behavior of the static dielectric function and the predicted screening properties of the system.

The qualitative behavior of the velocity autocorrelation function (VACF) can be well understood in terms of the dynamical charge and current fluctuation spectra. The VACF has also been found to exhibit a universal behavior.

[1] A. Melzer, V. A. Schweigert, I. V. Schweigert, A. Homann, S. Peters, and A. Piel, Phys. Rev. E **54**, R46 (1996). J. B. Pieper, J. Goree, and R. A. Quinn, J. Vac. Sci. Technol. **14**, 519 (1996); M. Zuzic, A. V. Ivlev, J. Goree, G. E. Morfill, H. M. Thomas, H. Rothermel, U. Konopka, R. Sutterlin, and D. D. Goldbeck, Phys. Rev. Lett. **85**, 4064 (2000); S. Robertson, A. A. S. Gulbis, J. Collwell, and M. Horányi, Phys. Plasmas **10**, 3874 (2003); Z. Sternovsky, M. Lampe, S. Robertson, IEEE Trans. Plasma Sci. **32**, 632 (2004).

[2] E. Grun, H. A. Zook, M. Gabuhl *et al.*, Nature (London) **362**, 428 (1993); H. Kruger, M. Horányi, and E. Grun, Geophys. Res. Lett. **30**, art. 1058 (2003); C. E. Krauss, M. Horányi, and S. Robertson, New J. Phys. **5**, art. 70 (2003).

[3] H. Löwen, J. Phys. A **36**, 5827 (2003); A. P. Hynninen and M. Dijkstra, J. Phys.: Condens. Matter **15**, S3557 (2003); S. Auer and D. Frenkel, *ibid.* **14**, 7667 (2002).

[4] C. C. Grimes and G. Adams, Phys. Rev. Lett. **36**, 145 (1976).

[5] R. C. Gann, S. Chakravarty, and G. V. Chester, Phys. Rev. B **20**, 326 (1979).

[6] R. K. Kalia, P. Vashishta, and S. W. de Leeuw, Phys. Rev. B **23**, 4794 (1981).

[7] H. Totsuji, C. Totsuji, and K. Tsuruta, Phys. Rev. E **64**, 066402 (2001).

[8] S. Nunomura, D. Samsonov, and J. Goree, Phys. Rev. Lett. **84**, 5141 (2000); V. Nosenko, S. Nunomura, and J. Goree, *ibid.* **88**, 215002 (2002); S. Nunomura, J. Goree, S. Hu, X. Wang, and A. Bhattacharjee, Phys. Rev. E **65**, 066402 (2002); H. Thomas, G. E. Morfill, V. Demmel, J. Goree, B. Feuerbacher, and D. Mohlmann, Phys. Rev. Lett. **73**, 652 (1994); S. K. Zhdanov, D. Samsonov, and G. E. Morfill, Phys. Rev. E **66**, 026411 (2002).

[9] M. S. Murillo and D. O. Gericke, J. Phys. A **36**, 6273 (2003).

[10] H. Totsuji, M. S. Liman, C. Totsuji, and K. Tsuruta, Phys. Rev. E **70**, 016405 (2004).

[11] G. J. Kalman, P. Hartmann, Z. Donkó, and M. Rosenberg, Phys. Rev. Lett. **92**, 065001 (2004).

[12] Z. Donkó, P. Hartmann, and G. J. Kalman, Phys. Rev. E **69**, 065401(R) (2004).

[13] H. Löwen, J. Phys. C **4**, 10105 (1992).

[14] G. E. Morfill, H. M. Thomas, U. Konopka, and M. Zuzic, Phys. Plasmas **6**, 1769 (1999).

[15] F. M. Peeters and X. Wu, Phys. Rev. A **35**, 3109 (1987).

[16] R. W. Hockney and J. W. Eastwood, *Computer Simulation Using Particles* (McGraw-Hill, New York, 1981).

[17] N. David and S. M. Hooker, Phys. Rev. E **68**, 056401 (2003).

[18] D. Frenkel and B. Smit, *Understanding Molecular Dynamics Simulations* (Academic, New York, 2001).

[19] P. Hopkins, A. J. Archer, and R. Evans, Phys. Rev. E **71**, 027401 (2005).

[20] J.-P. Hansen, I. R. McDonald, and E. L. Pollock, Phys. Rev. A **11**, 1025 (1975).

[21] S. Hamaguchi, Plasmas Ions **2**, 57 (1999).

[22] Y. Rosenfeld, J. Phys.: Condens. Matter **13**, L39 (2001).

[23] H. Ohta and S. Hamaguchi, Phys. Plasmas **7**, 4506 (2000).

[24] T. Saigo and S. Hamaguchi, Phys. Plasmas **9**, 1210 (2002).

[25] O. Vaulina, S. Khrapak, and G. Morfill, Phys. Rev. E **66**, 016404 (2002).

[26] O. Vaulina and S. V. Vladimirov, Phys. Plasmas **9**, 835 (2002).

[27] V. E. Fortov, O. S. Vaulina, O. F. Petrov, V. I. Molotkov, A. M. Lipaev,V. M. Torchinsky, H. M. Thomas, G. E. Morfill, S. A. Khrapak, Yu. P. Semenov, A. I. Ivanov, S. K. Krikalev, A. Yu. Kalery, S. V. Zaletin, and Yu. P.. Gidzenko, Phys. Rev. Lett. **90**, 245005 (2003).

[28] G. Faussurier and M. S. Murillo, Phys. Rev. E **67**, 046404 (2003).

[29] G. Faussurier, Phys. Rev. E **69**, 066402 (2004).

[30] H. Ikezi, Phys. Fluids **29**, 1764 (1986).

[31] S. Hamaguchi, R. T. Farouki, and D. H. E. Dubin, Phys. Rev. E **56**, 4671 (1997).

[32] K. I. Golden, G. Kalman, and P. Wyns, Phys. Rev. A **46**, 3463 (1992).

[33] S. T. Chui, Phys. Rev. Lett. **48**, 933 (1982); G. Aeppli and R. Bruinsma, *ibid.* **53**, 2133 (1984); K. J. Strandburg, Rev. Mod. Phys. **60**, 161 (1988); Ch. Simon, I. Rosenman, F. Batallan, C. Lartigue, and J. F. Legrand, Phys. Rev. B **45**, 2694 (1992); V. N. Ryzhov and E. E. Tareyeva, *ibid.* **51**, 8789 (1995).

[34] J. M. Kosterlitz and D. J. Thouless, J. Phys. C **6**, 1181 (1973).

[35] B. I. Halperin and D. R. Nelson, Phys. Rev. Lett. **41**, 121 (1978).

[36] I. V. Schweigert, V. A. Schweigert, and F. M. Peeters, Phys. Rev. Lett. **82**, 5293 (1999).

[37] K. I. Golden, H. Mahassen, and G. J. Kalman, Phys. Rev. E **70**, 026406 (2004).

[38] S. Kyrkos and G. J. Kalman, J. Phys. A **36**, 6235 (2003).

[39] J. P. Hansen, I. R. McDonald, and E. L. Pollock, Phys. Rev. A **11**, 1025 (1975).

[40] R. K. Kalia, P. Vashishta, S. W. de Leeuw, and A. Rahman, J. Phys. C **14**, L991 (1981).

[41] J. P. Hansen, D. Levesque, and J. J. Weis, Phys. Rev. Lett. **43**, 979 (1979).

[42] K. I. Golden and G. J. Kalman, Phys. Plasmas **7**, 14 (2000).

[43] P. Schmidt, G. Zwicknagel, P.-G. Reinhard, and C. Toepffer, Phys. Rev. E **56**, 7310 (1997).